

# Seasonal climate summary for the southern hemisphere (summer 2017–18): an exceptionally warm season for Australia – a short-lived and weak La Niña

Tamika Tihema

Bureau of Meteorology, GPO Box 413, Brisbane, Qld 4001, Australia.  
Email: tamika.tihema@bom.gov.au

**Abstract.** This is a summary of the southern hemisphere atmospheric circulation patterns and meteorological indices for summer 2017–18; an account of seasonal rainfall and temperature for the Australian region is also provided. A short-lived and weak La Niña developed but decayed by the end of February 2018. Sea-surface temperatures were exceptionally warm in the Tasman Sea from late 2017 to early 2018. It was an exceptionally warm summer for Australia, and the third-warmest mean temperature on record for the nation. Summer rainfall was close to the long-term average for Australia, with above-average rainfall in west and below-average rainfall in the east.

Received 13 August 2019, accepted 27 September 2019, published online 11 June 2020

## 1 Introduction

This summary reviews the southern hemisphere and equatorial climate patterns for summer 2017–18, with attention given to the Australasian and equatorial regions of the Pacific and Indian Ocean basins. The main sources of information for this report are analyses prepared by the Australian Bureau of Meteorology.

The national mean temperature for summer 2017–18 was the third-warmest on record. The mean maximum and mean minimum temperatures were the third and second warmest on record respectively. For Australia as a whole, in terms of mean temperature, December 2017 was the second warmest on record, followed by the second-warmest January and the equal ninth-warmest February.

Sea-surface temperatures (SSTs) in the Tasman Sea were exceptionally warm starting from late spring in 2017 through summer 2017–18, and a prolonged warm spell occurred in November 2017 in Tasmania and Victoria, coincided with an extended period of blocking high pressure in the south Tasman Sea. A Special Climate Statement,<sup>1</sup> jointly written by the National Institute of Water and Atmospheric Research, New Zealand (NIWA), and the Bureau of Meteorology (BoM), was published regarding the extreme marine heatwave in the Tasman Sea.

Rainfall was below average for most of eastern Australia and above average in Western Australia and the top end of the Northern Territory. There were five tropical cyclones that developed in or affected the Australian North-west Region during summer: *Dahlia*, *Hilda*, *Joyce*, *Irving* and *Kelvin* and

three (*Hilda*, *Joyce* and *Kelvin*) made landfall along the north-west coast of Australia.

## 2 Pacific and Indian Ocean basin climate indices

### 2.1 Southern Oscillation Index

The Troup Southern Oscillation Index<sup>2</sup> (SOI) for January 2014 to March 2018 is shown in Fig. 1, also shown is a 5-month weighted moving average of the monthly SOI. Sustained

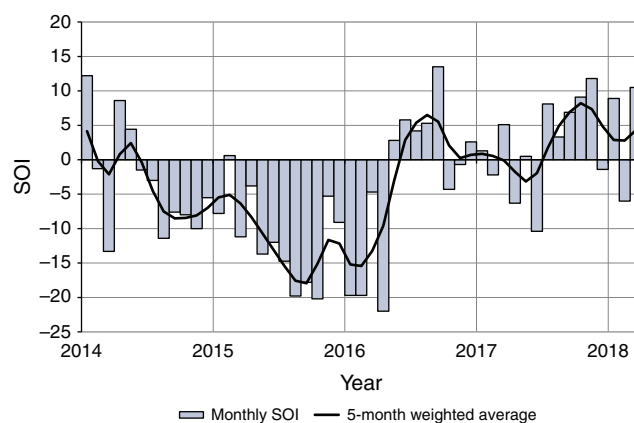


**Fig. 1.** Troup Southern Oscillation Index (SOI) values from January 2014 to March 2018, with a 5-month binomial weighted moving average.

<sup>1</sup><http://www.bom.gov.au/climate/current/statements/scs64.pdf>, verified 29 April 2020.

<sup>2</sup>The Troup Southern Oscillation Index (Troup 1965) used in this article is 10 times the standardised monthly anomaly of the difference in mean sea level pressure (MSLP) between Tahiti and Darwin. The calculation is based on 60-year climatology (1933–92), with records commencing in 1876. The Darwin MSLP is provided by the Bureau of Meteorology, and the Tahiti MSLP is provided by Météo France inter-regional direction for French Polynesia.

negative values of SOI below  $-7$  are often indicative of El Niño episodes, whereas persistently positive values of SOI above seven ( $+7$ ) are typical of a La Niña episode.

Following a rapid rise to a positive SOI value in July 2017, SOI values peaked at 11.8 in November 2017, then oscillated from  $-1.4$  in December, 8.9 in January then  $-6.0$  in February. A weak and short-lived La Niña developed late in 2017 and became established in the tropical Pacific  $\sim$ December 2017 to late February 2018. The event officially ended in March as El Niño–Southern Oscillation (ENSO) indicators returned to neutral levels or below La Niña thresholds.

## 2.2 Composite monthly El Niño–Southern Oscillation index (5VAR)

The ENSO 5VAR Index (5VAR<sup>3</sup>) is a composite monthly ENSO index, calculated as the standardised amplitude of the first principal component of the monthly Darwin and Tahiti mean sea level pressure (MSLP) and monthly indices NINO3, NINO3.4 and NINO4 SSTs.<sup>4</sup> Positive 5VAR values that are in excess of one standard deviation are typically associated with El Niño, whereas negative 5VAR values of a similar magnitude are indicative of La Niña. The NINO3.4 index, which measures SSTs in the central Pacific Ocean between  $5^{\circ}\text{N}$ – $5^{\circ}\text{S}$  and  $120$ – $170^{\circ}\text{W}$ , is used by the Australian Bureau of Meteorology to monitor ENSO; NINO3.4 is closely related to the Australian climate (Wang and Hendon 2007).

Fig. 2 shows 5VAR values all reached La Niña thresholds during the summer, being  $-0.305$  in December 2017,  $-0.733$  in January and then  $-0.413$  in February 2018. In fact, the sustained negative 5VAR values began earlier in September 2017 and lasted until April 2018.

## 3 Outgoing longwave radiation

Outgoing longwave radiation (OLR) in the equatorial Pacific Ocean can be used as an indicator of enhanced or suppressed tropical convection. Positive OLR anomalies typify a regime of reduced convective activity, a reduction in cloudiness and, usually, rainfall. Conversely, negative OLR anomalies indicate enhanced convection, increased cloudiness and chances of increased rainfall. During La Niña, decreased convection (positive OLR anomalies) can be seen near the Date Line, whereas increased cloudiness (negative OLR anomalies) near the Date Line usually occurs during El Niño.

Seasonal spatial patterns of OLR anomalies across the Asia-Pacific region between  $40^{\circ}\text{S}$  and  $40^{\circ}\text{N}$  for summer 2017–18 are shown in Fig. 3. Strong negative OLR anomalies were observed across north-west and central Western Australia, associated with the passage of a number of tropical cyclones in December (*Hilda*), January (*Joyce*) and February (*Kelvin*). The positive OLR anomalies (indicating reduced convection) are observed over the much of Queensland, reflecting the rainfall deficiency for the season. These positive anomalies extended into the

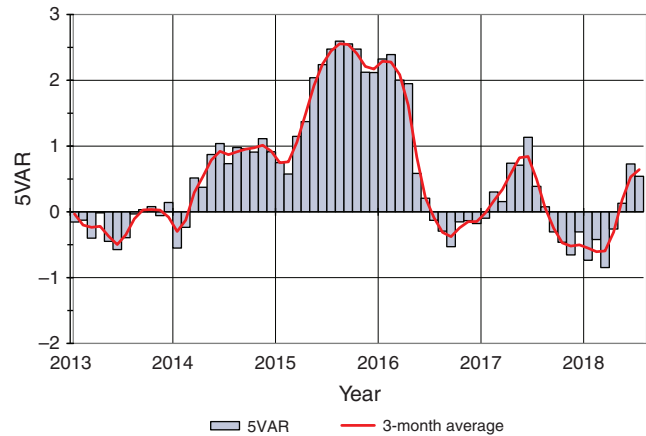


Fig. 2. Anomalies of the composite 5VAR El Niño–Southern Oscillation (ENSO) index for the period January 2013 to July 2018 with the 3-month binomially weighted moving average.

western tropical Pacific Ocean, the central India Ocean and also across the Tasman Sea near New Zealand.

However, there were suspected negative biases in the OLR anomalies over subtropical land areas (estimated at  $\sim 5 \text{ W m}^{-2}$ ) due to satellite orbit decay (Wheeler pers. comm.). Figure 4 is a map of the seasonal precipitation anomalies as calculated from NOAA's Climate Anomaly Monitoring System-Outgoing longwave radiation Precipitation Index (CAMS\_OPI) analysis for the Pacific region.

Precipitation was drier than average for the season for most of eastern Australia, across the central equatorial Pacific Ocean and in parts of eastern Peru and eastern Argentina, and wetter than average in Western Australia and parts of Indonesia, and also in parts of Chile and Bolivia.

## 4 Madden–Julian Oscillation

The Madden–Julian Oscillation (MJO) is a tropical convective wave anomaly that develops in the Indian Ocean and propagates eastwards into the Pacific Ocean. The MJO recurs approximately every 30 to 60 days (Madden and Julian 1971, 1972, 1994). When the MJO is in an active phase, it is associated with the areas of increased and decreased tropical convection, with effects on the southern hemisphere often weakening during early autumn, before transitioning to the northern hemisphere. A description of the Real-time Multivariate MJO (RMM) index and the associated phases can be found in Wheeler and Hendon (2004).

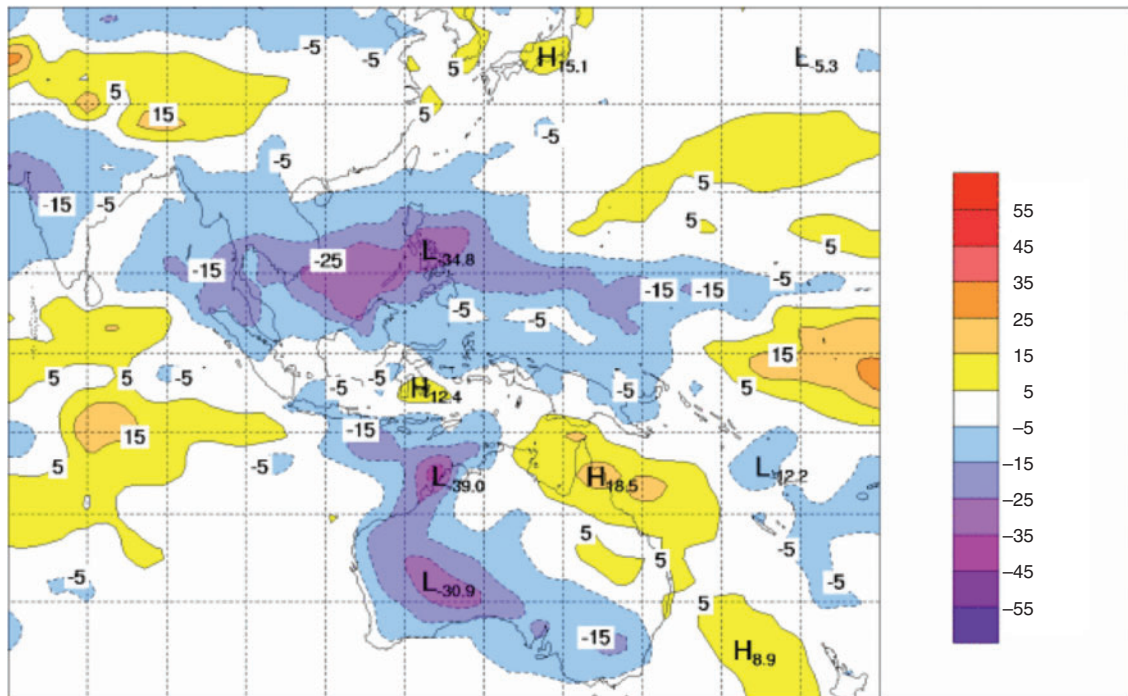
The phase-space diagram of the RMM for December 2017 to February 2018 is shown in Fig. 5.

A moderate to strong MJO pulse occurred in the Maritime Continent (phases 4 and 5) in late November and early December 2017, coinciding with tropical cyclone activity in the Indian Ocean. A moderate MJO travelled through the Indian Ocean and

<sup>3</sup> ENSO 5VAR was developed by the Bureau of Meteorology and is described by Kuleshov *et al.* (2009). The principal component analysis and standardisation of this ENSO index is performed over the period 1950–99.

<sup>4</sup> SST indices obtained from <ftp://ftp.cpc.ncep.noaa.gov/wd52dg/data/indices/sstoi.indices>, verified 29 April 2020.

OLR 2.5 x 2.5 NOAA REAL TIME-OLRAV (W/M<sup>-2</sup>) 20171201 0000 20180217 0000



© Commonwealth of Australia 2018, Australian Bureau of Meteorology

Issued: 01/03/2018

**Fig. 3.** The outgoing longwave radiation (OLR) anomalies for summer 2017–18 ( $W m^{-2}$ ). Anomalies calculated with respect to the base period 1979–2000. There are suspected negative biases in the OLR anomalies over subtropical land areas (estimated at  $\sim 5 W m^{-2}$ ) due to satellite orbit decay.

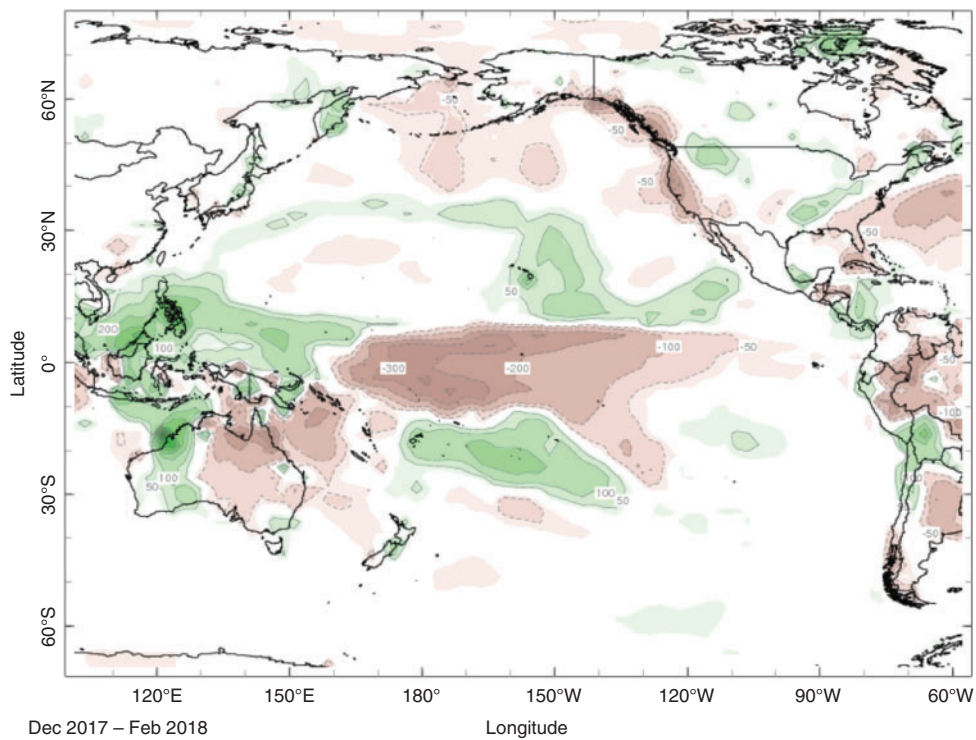


**Fig. 4.** Precipitation anomalies for summer 2017–18 (mm/season) for the Pacific region. Base period is 1979–2000.

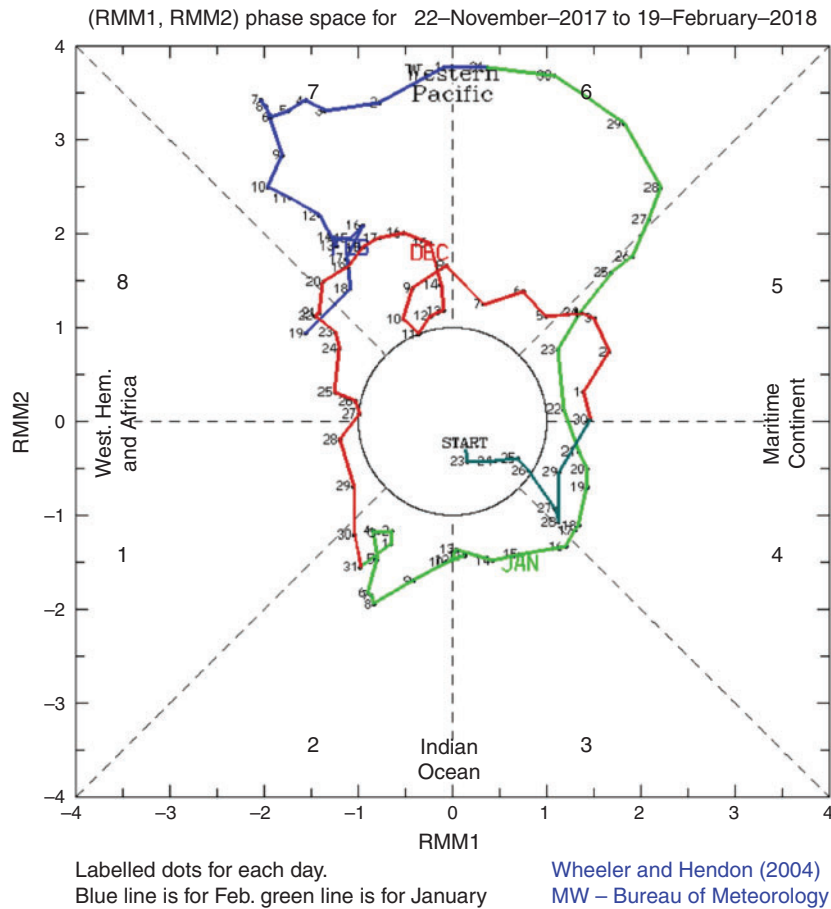


**Fig. 5.** Phase-space representation of the Madden–Julian Oscillation (MJO) index for December 2017 to February 2018, daily values are shown with December in red, January in green and February in blue. The eight phases of the MJO and the corresponding (approximate) locations of the near-equatorial enhanced convective signal are labelled.

Maritime Continent (phases 2–5) throughout January and became a strong pulse in the western Pacific regions (phases 6 and 7) in late January to mid-February, which coincided with an active monsoon trough over northern Australia.

The Hovmöller diagram of OLR anomalies along the equator during 16 October 2017 to 16 April 2018 (Fig. 6) shows the progress of MJO. There were two clear bursts of eastward-moving convection during late spring and summer; with negative OLR anomalies traversed from 80 to 120°E in late November to early December, and another from the start of January into February.

## 5 Oceanic patterns

### 5.1 Sea-surface temperatures

Fig. 7 shows the global sea-surface temperature (SST) for the combined ocean area of the southern hemisphere for summer 2017–18.<sup>5</sup> SSTs were more than one degree above average over much of the Tasman Sea and western Pacific, across northern Australia. SST anomalies of more than two degrees above

average were evident between New Zealand and south-east Australia (Fig. 7).

The notable high SSTs in the southern Tasman Sea were exceptionally high in late 2017. The high temperatures extended west from New Zealand to Tasmania and mainland south-east Australia. The temperatures exceeded previously observed values at the time of year in the region. A joint Special Climate Statement was released by the BoM and the National Institute of Water and Atmospheric Research (NIWA), titled ‘Special Climate Statement–record warmth in the Tasman Sea, New Zealand and Tasmania’ (<http://www.bom.gov.au/climate/current/statements/scs64.pdf>, accessed 29 April 2020).

Blocking high-pressure systems over south-east Australia in October and November saw sunny conditions and suppressed cloud cover over the Tasman Sea. The persistent highs led to warmer than average SSTs extending across the Tasman Sea between southern Australia and New Zealand from November 2017. The monthly SST decile maps are shown in Fig. 8 for December 2017,

<sup>5</sup>NOAA National Centers for Environmental information, Climate at a Glance: Global Time Series, published May 2017, retrieved on 13 May 2017 from <http://www.ncdc.noaa.gov/cag/>, verified 29 April 2020 (base period 1900–present).

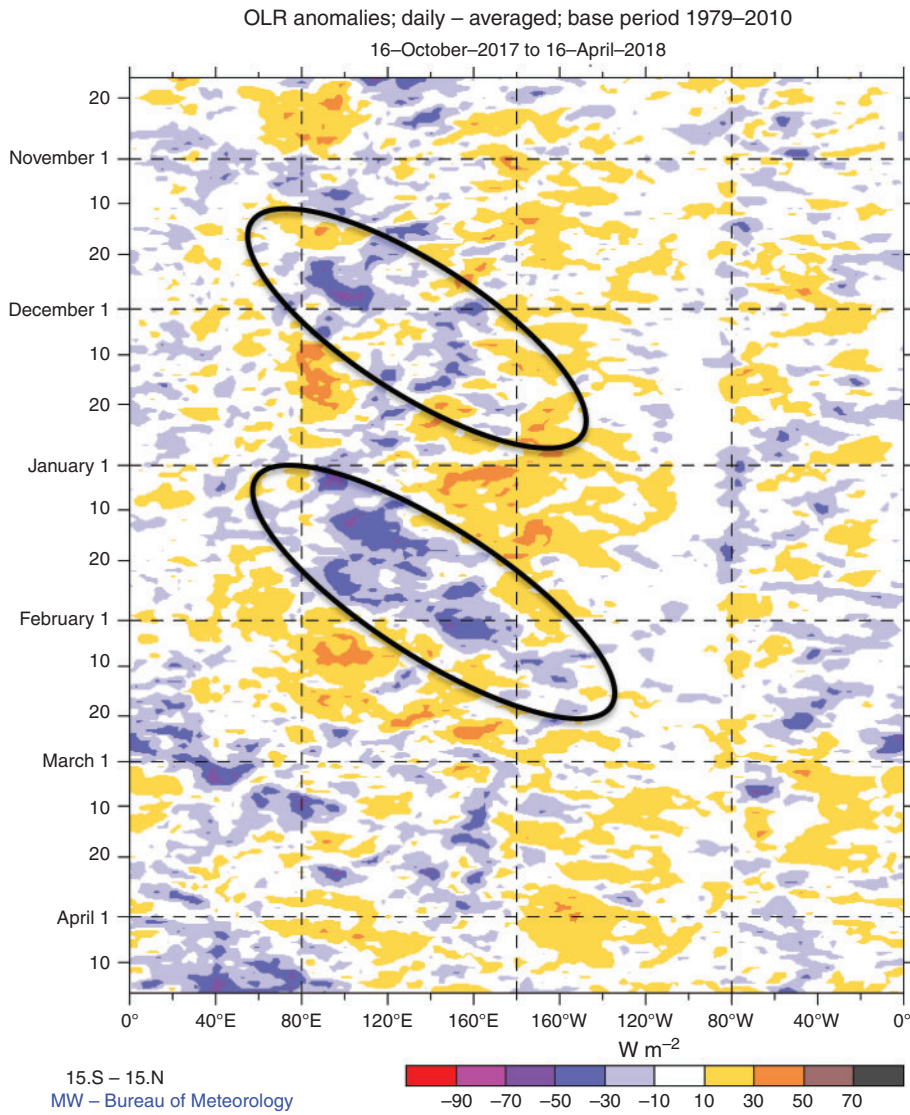


**Fig. 6.** Time-longitude plot of outgoing daily-averaged long-wave radiation (OLR) anomalies at the equator over the period October 2017 to April 2018. OLR anomaly is from daily data with respect to a base period of 1979–2010, using interpolated OLR data provided by the NOAA/OAR/ESRL PSD, Boulder, Colorado, USA.

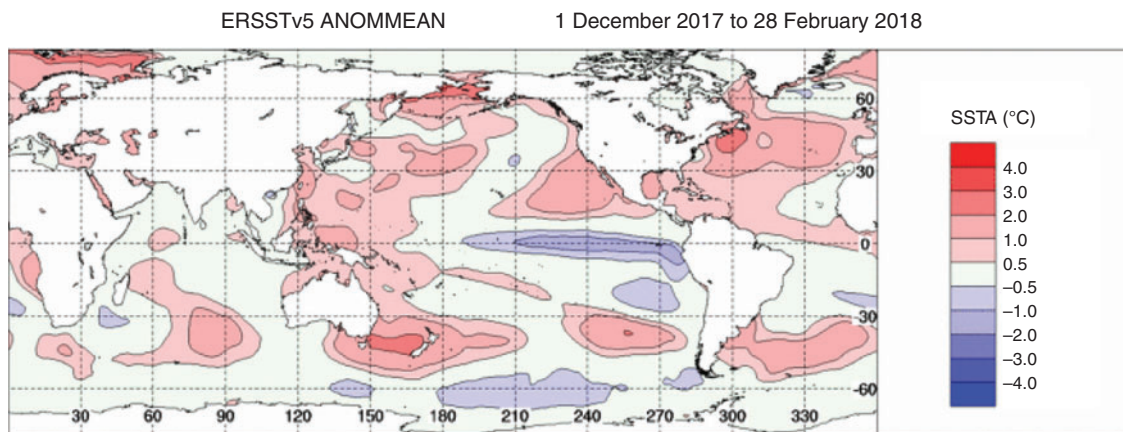
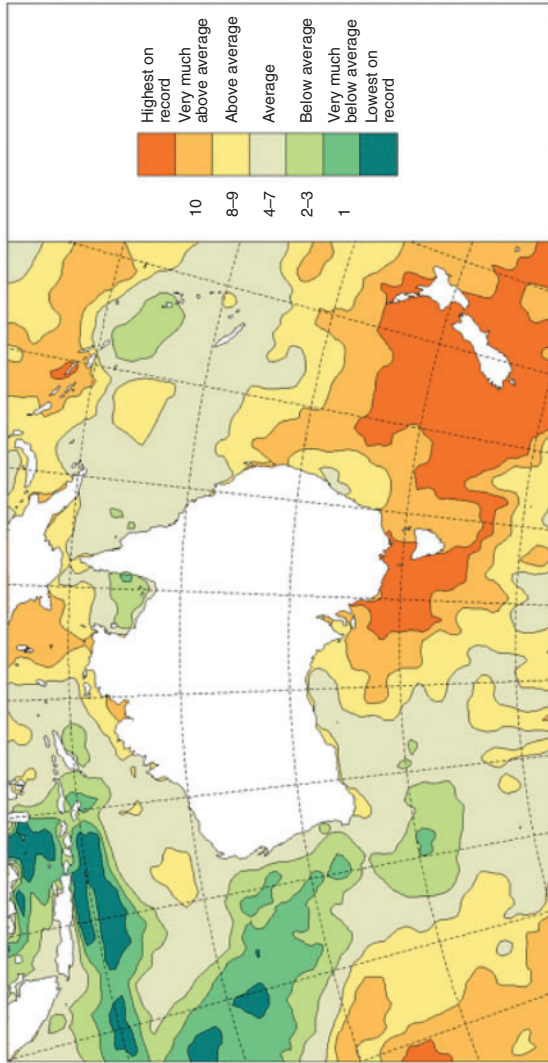


**Fig. 7.** Global sea-surface temperature anomaly (°C) for austral summer 2017–18 (Reynolds NCEP Global ERRSTv5).

REYN SST PERCENTILES  
1 December 2017 to 28 February 2018  
Distribution based on gridded data



Australian Region SST deciles 20171201 to 20171231 (Reynolds analysis)  
Distribution based on gridded data

Australian Region SST deciles 20180101 to 20180131 (Reynolds analysis)  
Distribution based on gridded data

Australian Region SST deciles 20180201 to 20180228 (Reynolds analysis)  
Distribution based on gridded data

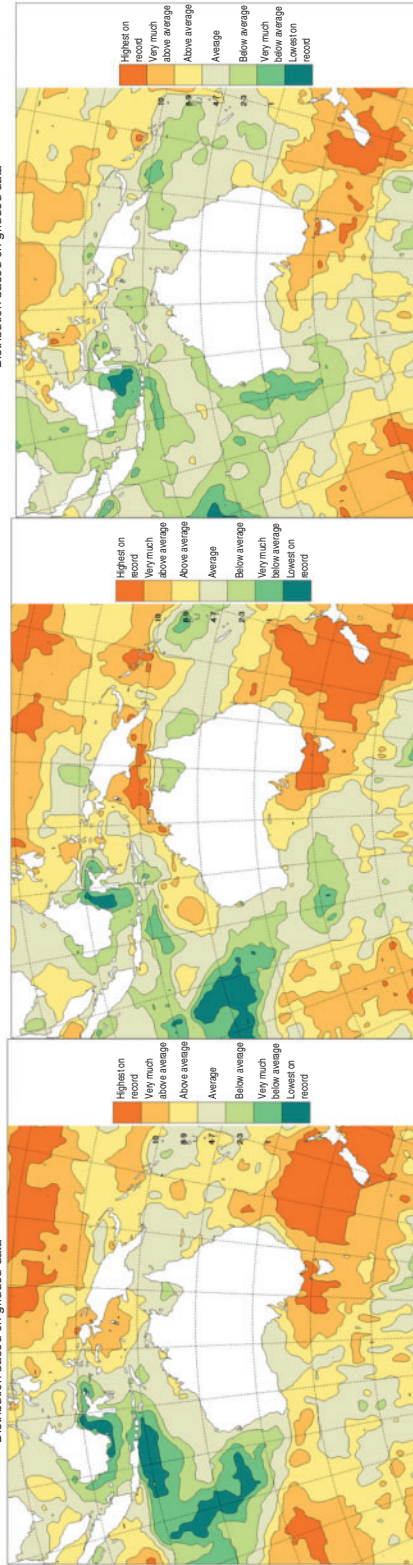
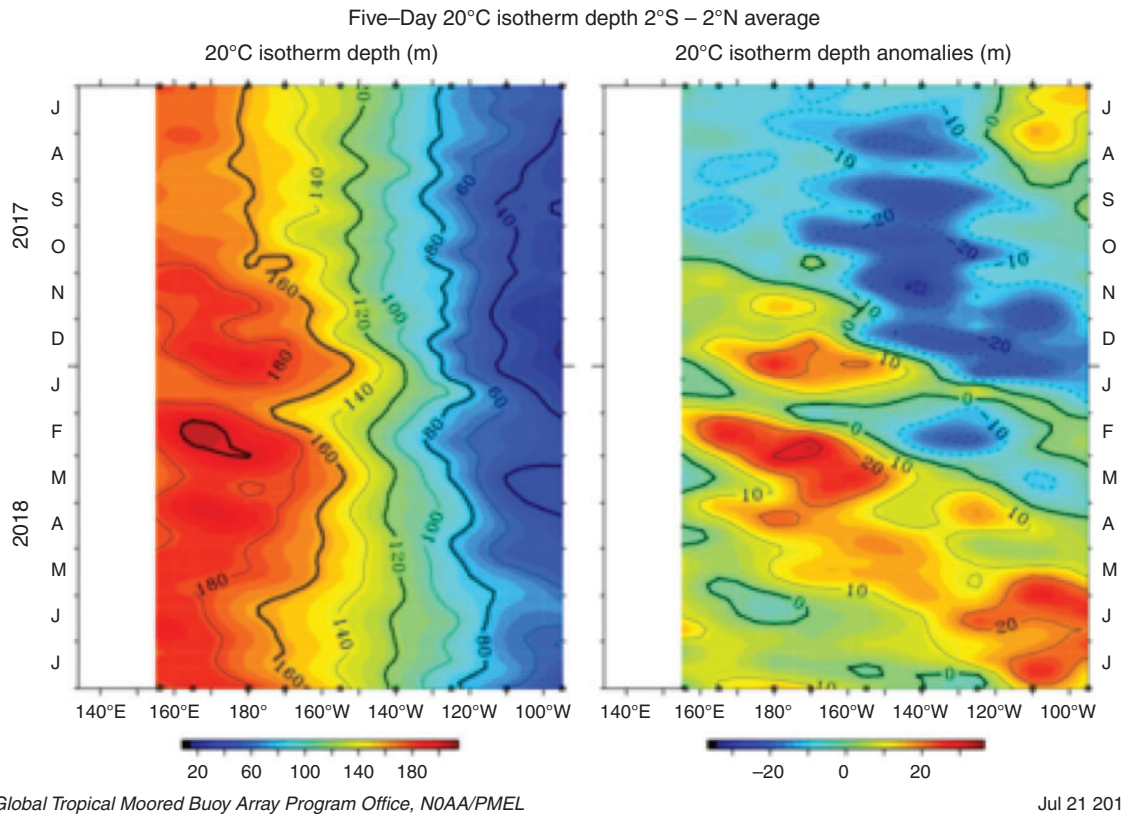


Fig. 8. Sea-surface temperature (SST) decile map of the Australian region for summer 2017–18 (upper panel), and for December 2017, January 2018 and February 2018 (lower panel).



**Fig. 9.** Hovmöller diagram of the 20°C isotherm depth and anomaly along the equator from July 2017 to July 2018, obtained from NOAA's TAO/TRITON data.<sup>6</sup>

January 2018 and February 2018 (bottom panel), as well as for the summer 2017–18 period (top panel). Record high SSTs were evident around south-east Australia and around Tasmania, and east to New Zealand in December and January, with SSTs cooled to below record high levels in many parts in February.

However, the SSTs maintained record-high levels to the south and east of New Zealand. This was mainly due to high MSLP in the east and south-east of New Zealand from January 2018 and lower than usual air pressures over the country and Tasman Sea.

### 5.2 Equatorial subsurface patterns

The 20°C isotherm depth is generally located close to the equatorial thermocline, which is the region of greatest temperature gradient with depth and is the boundary between the warm near-surface and cold deep-ocean waters. Measurements of the 20°C isotherm depth make a good proxy for the thermocline depth. Negative anomalies correspond to the 20°C isotherm being shallower than average and is indicative of a cooling of subsurface temperatures. If the thermocline anomaly is positive, the depth of the thermocline is deeper. A deeper thermocline results in less cold water available for upwelling, and therefore a warming of surface temperatures.

The Hovmöller diagram of the 20°C isotherm depth and anomaly along the equator from July 2017 to July 2018 (Fig. 9) shows negative anomalies across the equatorial Pacific through spring 2017, with warming in the western Pacific commencing in late October and persisting into summer 2017–18. This represents the thermocline deepening near the western Pacific over the summer into March 2018, and warmer temperatures at the surface.

Equatorial Pacific Ocean subsurface temperature anomalies from December 2017 to March 2018 (Fig. 10) show the fluctuations of warming and cooling in the central and eastern Pacific Ocean. The cool anomalies in the eastern Pacific are evident and consistent with a very weak La Niña pattern. The gradual warming in the western Pacific indicates the weakening and eventual dissipation of the La Niña event by March 2018.

## 6 Atmospheric circulation

### 6.1 Surface analyses

The MSLP pattern for summer 2017–18 is shown in Fig. 10, computed using data from the 0000 UTC daily analyses of the BoM's Australian Community Climate and Earth System Simulator (ACCESS) model.<sup>7</sup> MSLP anomalies are shown in

<sup>6</sup>Hovmöller plot obtained from <http://www.pmel.noaa.gov/tao/jsdisplay/>, verified 29 April 2020.

<sup>7</sup>For more information on the Bureau of Meteorology's ACCESS model, see <http://www.bom.gov.au/nwp/doc/access/NWPData.shtml>, verified 29 April 2020.

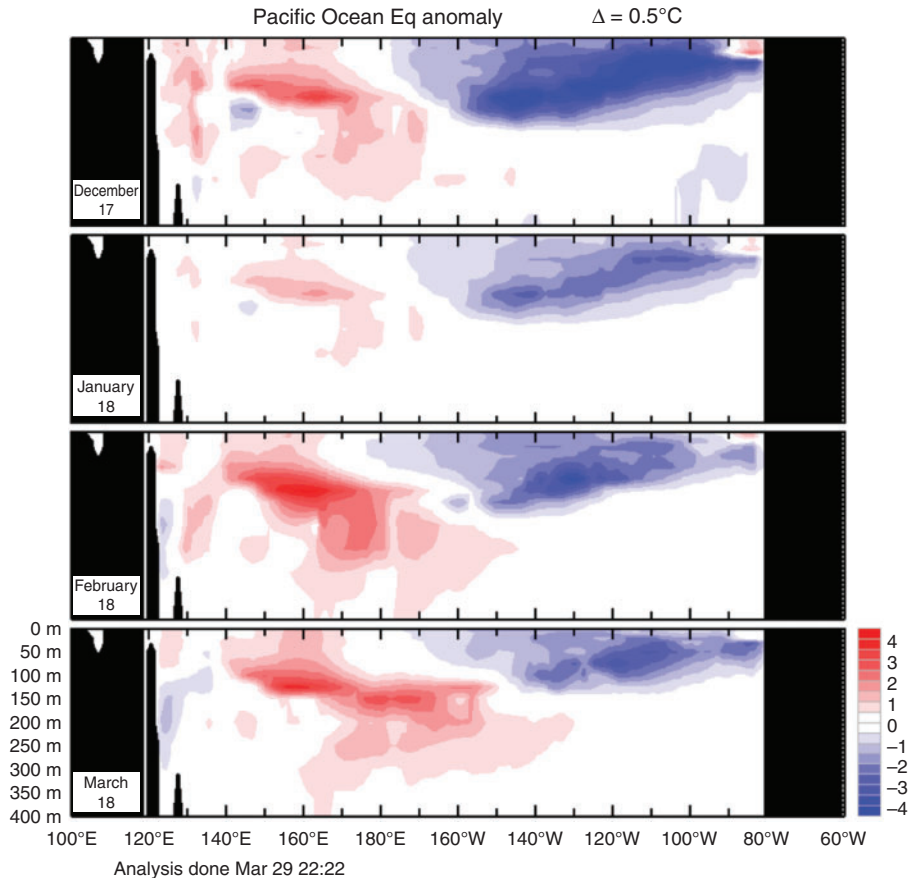


**Fig. 10.** The cross-section of monthly equatorial subsurface analysis from December 2017 to March 2018. Red shading indicates positive (warm) anomalies and blue shading indicates negative (cool) anomalies.

Fig. 11, relative to the 1979–2000 climatology obtained from the National Center for Environmental Prediction (NCEP) II Reanalysis data (Kanamitsu *et al.* 2002). The MSLP anomaly field is not shown over areas of elevated topography (grey shading).

The seasonal MSLP charts for the mean (Fig. 11) and anomalies (Fig. 12) show anomalously high pressure over Australia. Areas of higher than average pressure can also be seen at  $\sim 140^\circ\text{W}$  and  $\sim 80^\circ\text{E}$ , with anomalies of  $\sim +3.0$ -hPa east of New Zealand. Anomalously low pressure of  $-10.0$  hPa is evident at  $\sim 100^\circ\text{W}$ , and a band of anomalously low pressure of more than  $-5.0$  hPa from  $140$  to  $10^\circ\text{W}$ .

### 6.2 Mid-tropospheric analyses

The 500-hPa geopotential height, an indicator of the steering of surface synoptic systems across the southern hemisphere for summer 2017–18, is shown in Fig. 13. The associated anomalies, relative to the 1979–2000 climatology, are shown in Fig. 14. Geopotential height is valuable for identifying and locating features like troughs and ridges which are the upper level equivalents of surface low- and high-pressure systems respectively. Anomalously high geopotential height was observed across Australia, whereas in the east of New Zealand,

anomalies were slightly higher. A band of negative anomalies is evident over high latitudes and at longitudes of  $\sim 120$ – $90^\circ\text{W}$ .

## 7 Winds

Figures 15 and 16 show summer 2017–18 low-level (850 hPa) and upper level (200 hPa) wind anomalies respectively (winds computed from ACCESS and anomalies with respect to the 22-year 1979–2000 NCEP climatology). Isotach contours are at an interval of  $5 \text{ m s}^{-1}$ . At 850 hPa level, there are strongly westerly anomalies over mid- to high latitudes, with some regions more than  $5 \text{ m s}^{-1}$  above average. The pattern is also reflected in the upper level wind anomalies, with anomalies to the south of Australia more than  $20 \text{ m s}^{-1}$  above average.

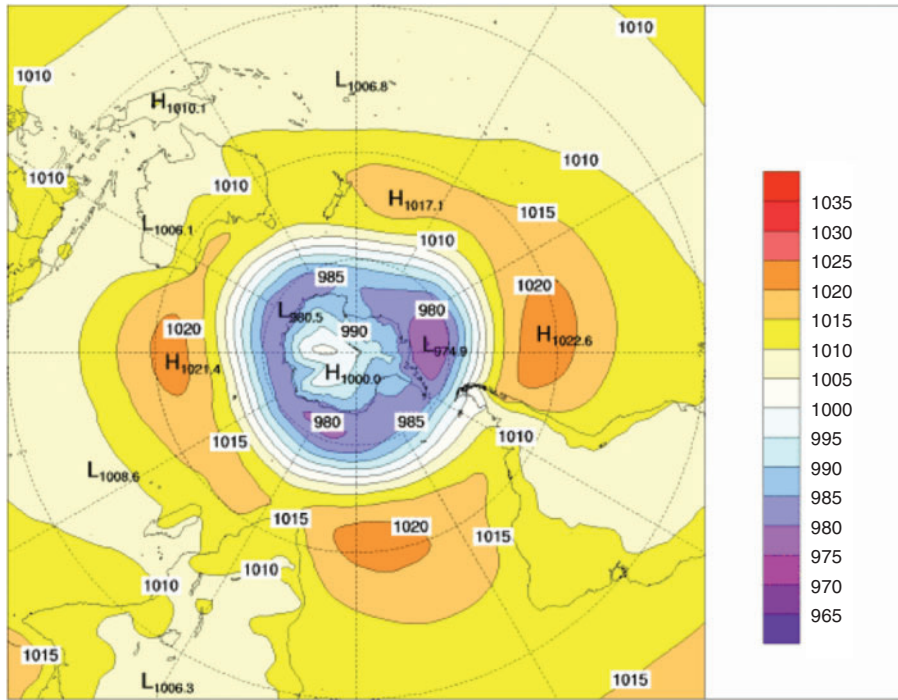
## 8 Australian region

### 8.1 Rainfall

Australian summer rainfall totals for 2017–18 are shown in Fig. 17a, with rainfall deciles shown in Fig. 17b. The deciles are calculated with respect to gridded rainfall data (Jones *et al.* 2009) for all summers between 1900–01 and 2017–18 (i.e. 118 summers).

Summer rainfall was near average for Australia as a whole. Rainfall was below average for the eastern half of the Northern

MSLP 2.5 × 2.5 ACCESS OP. ANAL. (hPa) 20171201 0000 20180228 0000

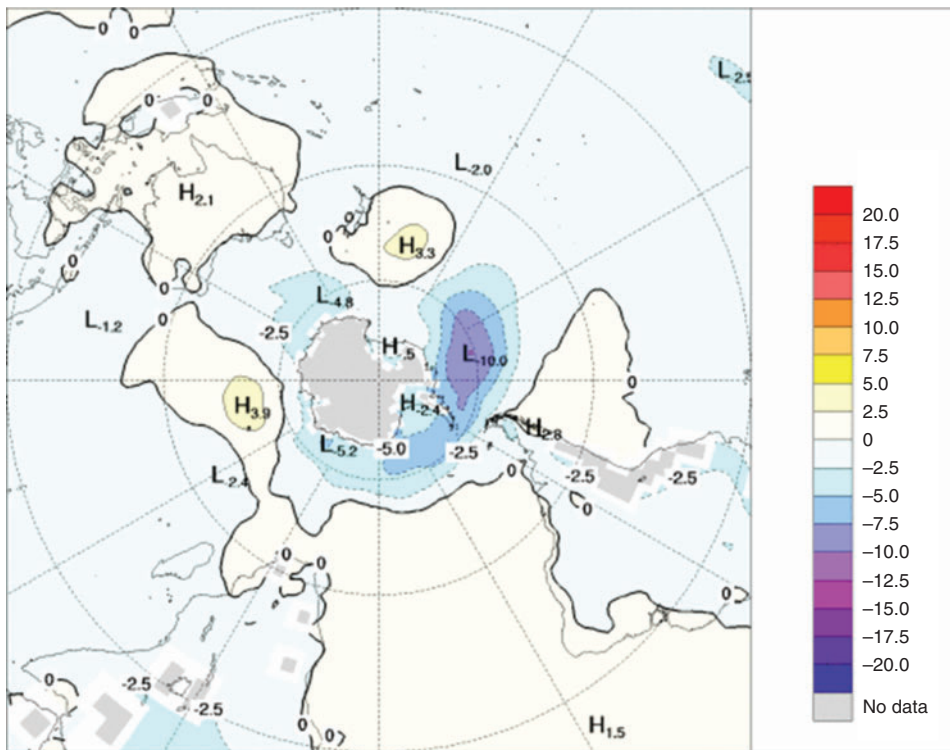


© Commonwealth of Australia 2018, Australian Bureau of Meteorology

Issued: 01/03/2018

Fig. 11. Southern hemisphere mean sea level pressure (MSLP) pattern for summer 2017–18.

MSLP 2.5 × 2.5 ACCESS OP. ANAL.-NCEP2 (hPa) 20171201 0000 20180228 0000

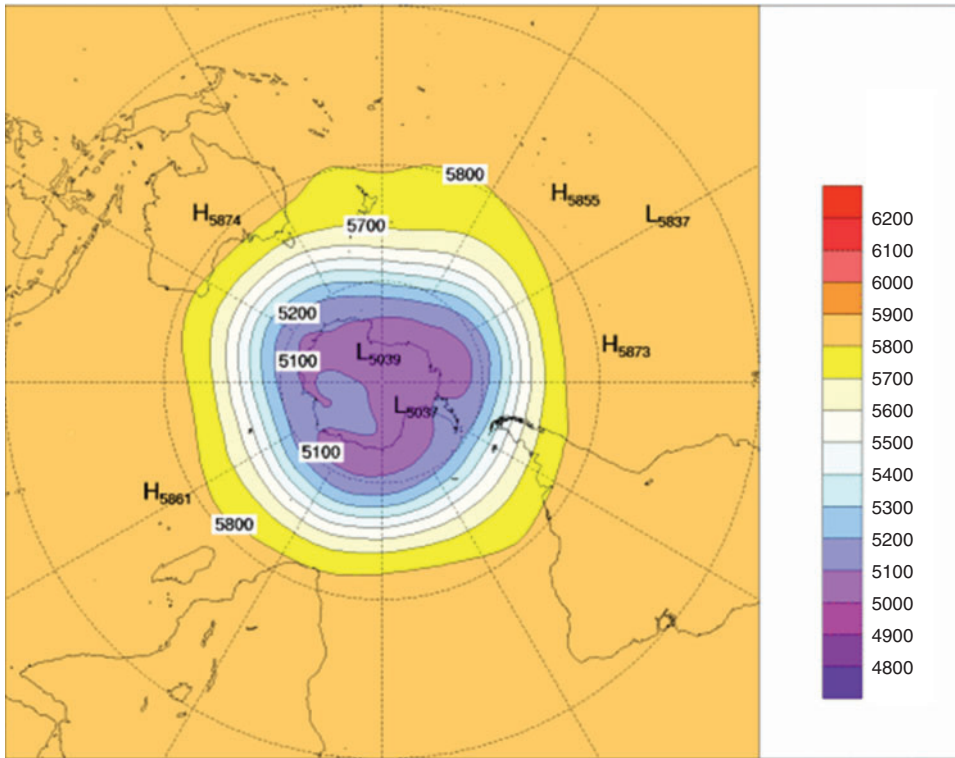


© Commonwealth of Australia 2018, Australian Bureau of Meteorology

Issued: 01/03/2018

Fig. 12. Southern hemisphere mean sea level pressure (MSLP) anomalies (hPa) for summer 2017–18. Anomalies calculated with respect to base period of 1979–2000.

Z0500 2.5 × 2.5 ACCESS OP. ANAL. (M) 20171201 0000 20180228 0000

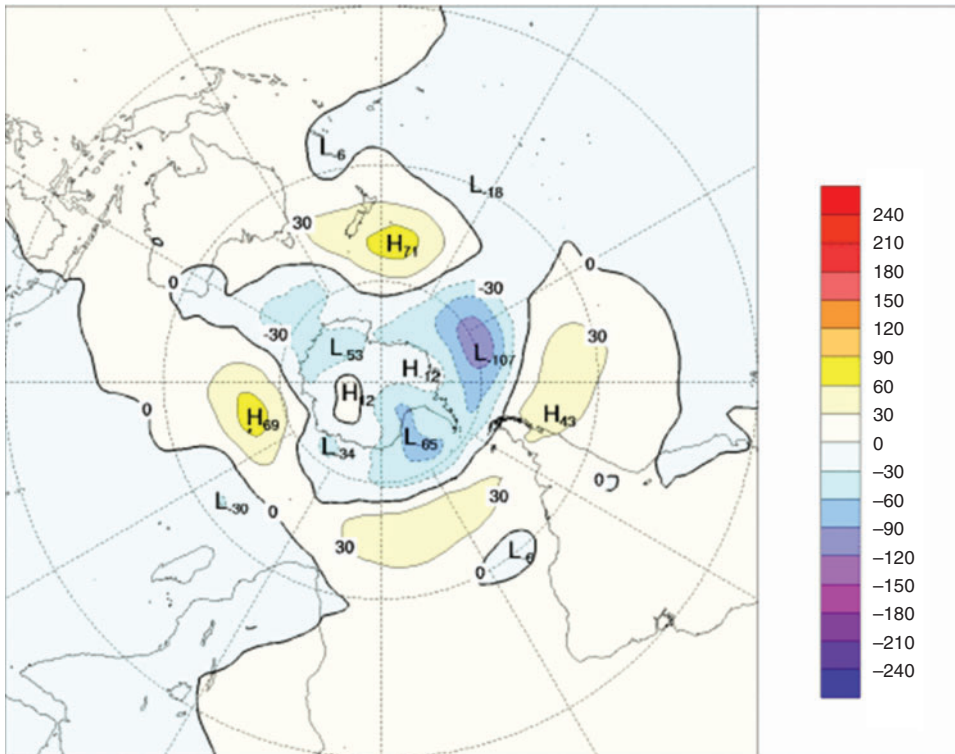


© Commonwealth of Australia 2018, Australian Bureau of Meteorology

Issued: 01/03/2018

**Fig. 13.** Summer 2017–18 500-hPa mean geopotential height (gpm).

Z0500 2.5 × 2.5 ACCESS OP. ANAL.-NCEP2 (M) 20171201 0000 20180228 0000

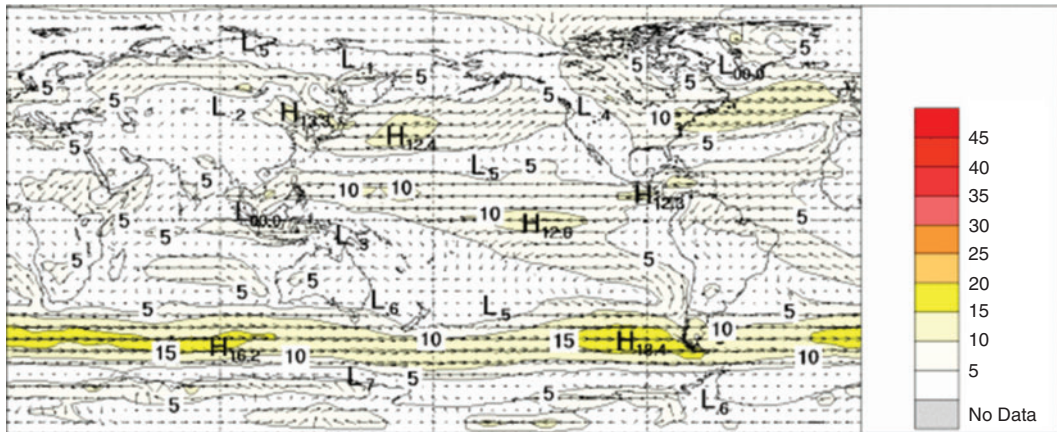


© Commonwealth of Australia 2018, Australian Bureau of Meteorology

Issued: 01/03/2018

**Fig. 14.** Summer 2017–18 500-hPa mean geopotential height anomalies (gpm) from 1979 to 2000 climatology.

IVI0850 2.5 × 2.5 ACCESS OP.ANAL. (M/S) 20171201 0000 20180228 0000

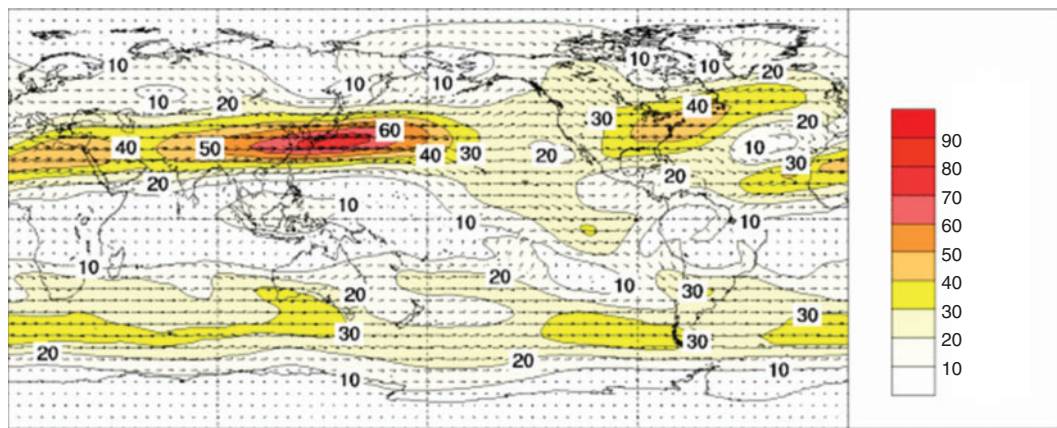


© Commonwealth of Australia 2018, Australian Bureau of Meteorology

Issued: 01/03/2018

Fig. 15. Austral summer 2017–18, 850 hPa vector wind anomalies ( $\text{m s}^{-1}$ ).

IVI0200 2.5 × 2.5 ACCESS OP.ANAL. (M/S) 20171201 0000 20180228 0000



© Commonwealth of Australia 2018, Australian Bureau of Meteorology

Issued: 01/03/2018

Fig. 16. Austral summer 2017–18, 200 hPa vector wind anomalies ( $\text{m s}^{-1}$ ).

Territory to the south of the Carpentaria forecast district, most of Queensland, parts of northern and eastern New South Wales, in the western half of Victoria and the far south-east of South Australia. Summer rainfall was in the lowest 10% of historical observations (decile 1) for much of central inland and western Queensland, with below-average rainfall over most of these regions for each month of summer. It was the driest summer on record for some stations in western and southern Queensland. Rainfall was above average for most of Western Australia, most of the top end of the Northern Territory, the western half of South Australia, much of southern New South Wales and most of the eastern half of Victoria.

Western Australia had its 10th-wettest summer on record. Several tropical lows and cyclones contributed to above-average monthly rainfall in Western Australia for each month of summer. Heavy rainfall accompanied tropical cyclone *Hilda* in December in the western Kimberley. In mid-January, the remnant low associated with tropical cyclone *Joyce* produced

very high monthly and seasonal rainfall totals along parts of the west coast of Australia, including in the Perth region. A tropical low tracked across the top end in the Northern Territory and the Kimberley in Western Australia in late January and contributed to a record wet January for some locations. During mid-February, tropical cyclone *Kelvin* brought very high daily rainfall totals to the Kimberley region. There was also record-breaking rain in the first 2 days of December in south-eastern Australia. A blocking high over the Tasman Sea drew moist tropical air into the south-east, with very heavy rain leading to high daily rainfall totals, some record high, in December in Victoria, southern New South Wales, and northern Tasmania. Table 1 shows a summary of seasonal rainfall ranks and extremes on a national and State basis for summer 2017–18.

### 8.2 Rainfall deficiencies

For the 9-month time period (1 June 2017 to 28 February 2018), serious to severe rainfall deficiencies were evident across large

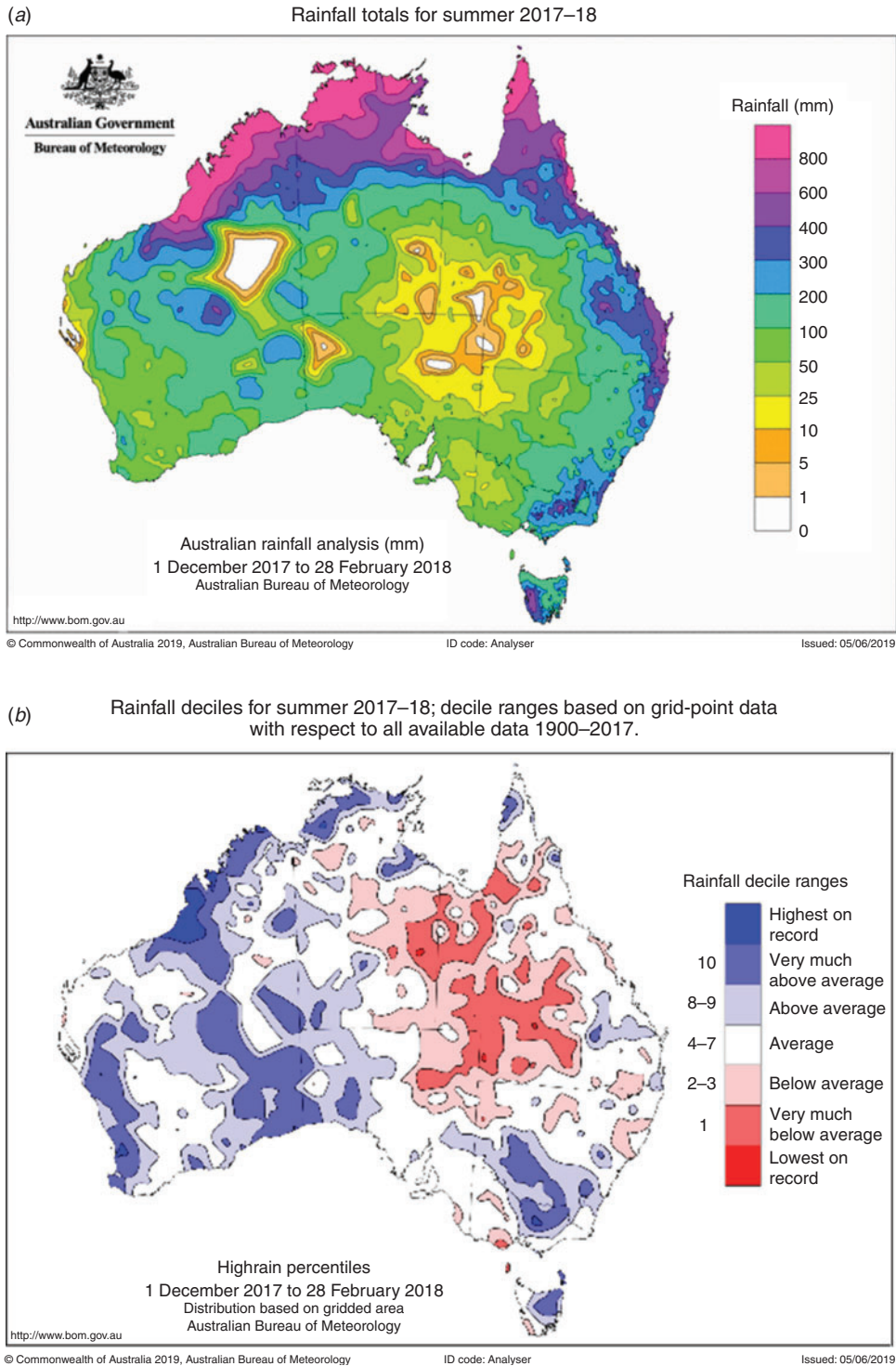


**Fig. 17.** (a) Rainfall totals for summer 2017–18. (b) Rainfall deciles for summer 2017–18; decile ranges based on grid-point data with respect to all available data 1900–2017.

areas of western to central and southern Queensland; in an area of eastern New South Wales affecting the Illawarra, Central Tablelands, Sydney, and Hunter regions; and in scattered

pockets of northern and western New South Wales. Serious or severe deficiencies were also observed across the Flinders Ranges in South Australia and along the east coast of Tasmania.

**Table 1. Summary of the seasonal rainfall ranks and extremes on a national and state basis for summer 2017–18**  
The rank refers to 1 (lowest)–119 (highest) and is calculated over the years 1900–2018 inclusive

Region	Highest seasonal total (mm)	Lowest seasonal total (mm)	Highest daily total (mm)	Area averaged total	Rank of area averaged total (mm)	Difference from mean (%)
Australia	1630.6 at Bellenden Ker (top)	Zero at several locations	380.6 at Mt Olive on 22 May	224.87	82	7.8
Queensland	1630.6 at Bellenden Ker (top)	Zero at several locations	380.6 at Mt Olive on 22 May	229.61	17	–29.3
New South Wales	542.0 at Murwillumbah (Dungay)	15.9 at Mogil Mogil (Benimora)	142.6 at Ourimbah (Dog Trap Road) on 28 March	132.14	45	–22.7
Victoria	456.2 at Toolangi	18.0 at Rainbow (Pigick)	182.2 at Gooram (Hillside) on 2 December 2017	127.60	73	6.7
Tasmania	724.4 at Mt Read	21.2 at Forthside Research Station	102.0 at Pyengana on 3 December 2017	240.66	54	–1.1
South Australia	121.2 at Parawa (Sharon)	Zero at several locations	54.0 at Boolcoomatta on 2 December 2017	66.65	85	7.5
Western Australia	1848.0 at Country Downs	zero at several locations	439.4 at Broome Airport on 30 January 2018	262.77	110	76.0
Northern Territory	1805.4 at Kangaroo Flats (Defence)	8.8 at Marqua	286.4 at Humpty Doo Collard Road on 28 January 2018	339.68	72	7.5

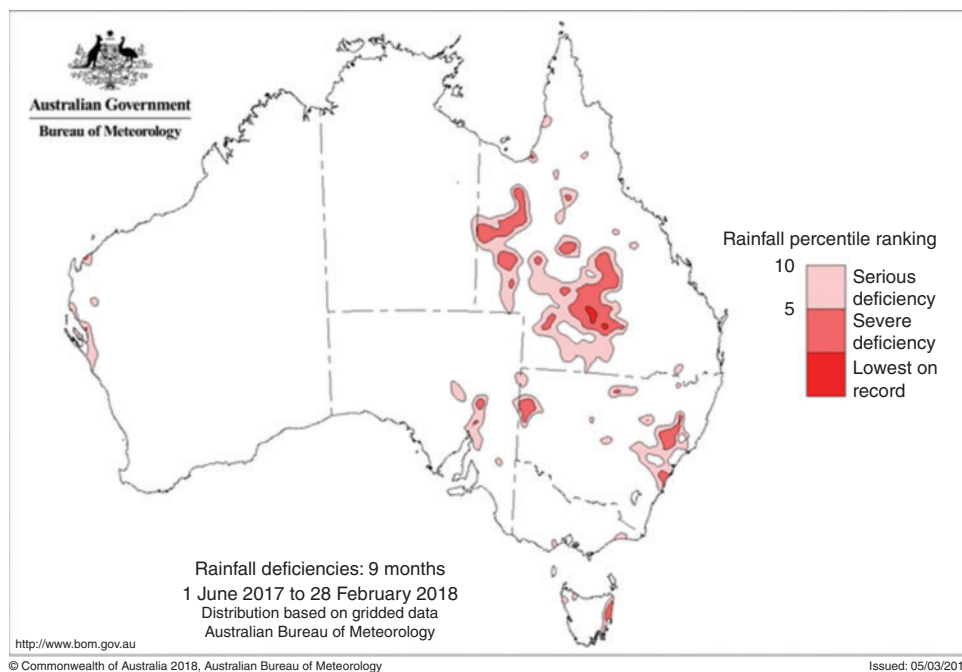


**Fig. 18.** Rainfall deficiencies for the 9-month period – June 2017 to February 2018.

In Western Australia, generally serious rainfall deficiencies were in place along the coastline around Shark Bay and Carnarvon. Figure 18 shows rainfall deficiencies at the 9-month period ending 28 February 2018. Table 2 shows the percentage area in different categories for June 2017 to February 2018.

For the 11-month time period (1 April 2017 to 28 February 2018), serious or severe rainfall deficiencies were present along the coast between around Onslow in the Pilbara and Cervantes in the Central West District. Isolated pockets of serious rainfall

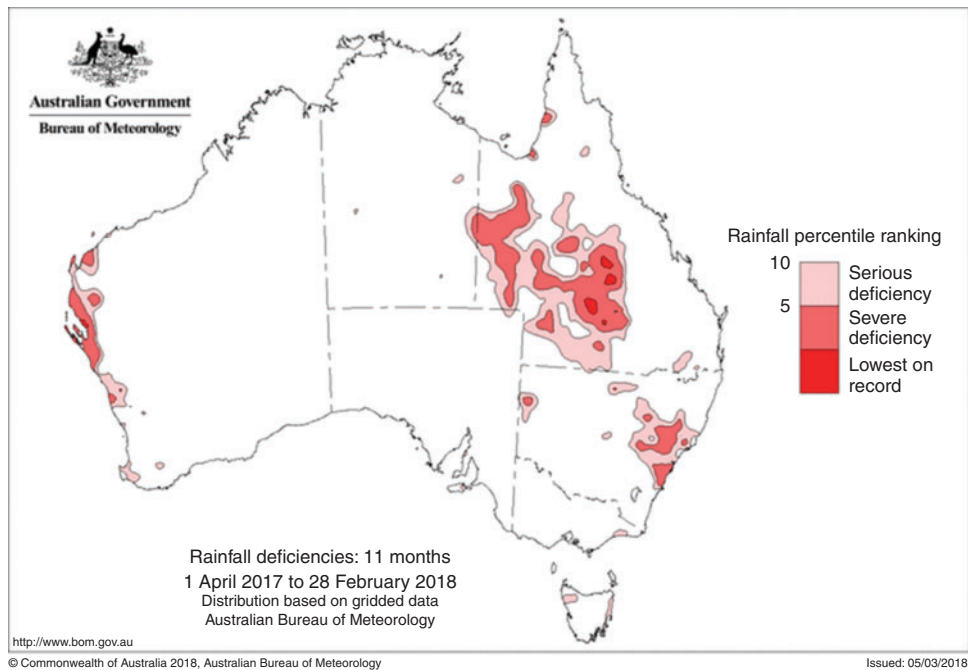
deficiencies were also analysed in the south-west. Figure 19 shows rainfall deficiencies for the 11-month period April 2017 to February 2018.

In eastern Australia, serious or severe rainfall deficiencies were observed across most of western to central inland Queensland, south of the Gulf Country, and a large area of eastern New South Wales reaching from the Illawarra to the Manning District on the coast, and extending inland towards Narrabri. Small patches of deficiencies were also present in central northern

**Table 2. Percentage areas in different categories for 9-month period (June 2017 to February 2018) rainfall**

'Severe deficiency' denotes rainfall at or below the 5th percentile. Areas in decile 1 include those in 'severe deficiency', which, in turn, includes areas which are 'lowest on record'. Areas in decile 10 include areas which are 'highest on record'. Percentage areas of highest and lowest on record are given to two decimal places because of the small quantities involved; other percentage areas are to one decimal place

Region	Lowest on record (%)	Severe deficiency (%)	Decile 1 (%)	Decile 10 (%)	Highest on record (%)
Australia	0.16	2.7	8.1	14.1	1.18
Queensland	0.69	8.4	22.8	0.2	0.00
New South Wales	0.00	3.8	12.9	0.0	0.00
Victoria	0.00	0.0	2.4	0.0	0.00
Tasmania	0.91	7.2	19.0	0.0	0.00
South Australia	0.00	1.6	7.5	23.0	0.14
Western Australia	0.00	0.3	1.1	29.1	3.24
Northern Territory	0.00	0.0	0.2	9.4	0.57

**Fig. 19.** Rainfall deficiencies for the 11-month period – April 2017 to February 2018.**Table 3. Percentage areas in different categories for April 2017 to February 2018 rainfall**

'Severe deficiency' denotes rainfall at or below the 5th percentile. Areas in decile 1 include those in 'severe deficiency', which, in turn, includes areas which are 'lowest on record'. Areas in decile 10 include areas which are 'highest on record'. Percentage areas of highest and lowest on record are given to two decimal places because of the small quantities involved; other percentage areas are to one decimal place

Region	Lowest on record (%)	Severe deficiency (%)	Decile 1 (%)	Decile 10 (%)	Highest on record (%)
Australia	0.29	4.6	11.4	14.1	1.23
Queensland	0.89	14.4	32.5	0.0	0.00
New South Wales	0.16	5.5	15.6	0.0	0.00
Victoria	0.00	0.0	1.6	0.0	0.00
Tasmania	0.00	0.9	12.7	0.0	0.00
South Australia	0.00	0.1	2.1	22.1	0.27
Western Australia	0.22	2.0	4.5	28.1	3.54
Northern Territory	0.00	0.2	2.6	11.9	0.23

**Table 4. Percentage areas in different categories for summer 2017–18**

Areas in decile 1 include those which are ‘lowest on record’. Areas in decile 10 include areas which are ‘highest on record’. Percentage areas of highest and lowest on record are given to two decimal places because of the small quantities involved; other percentage areas are to one decimal place

Region	Maximum temperature				Minimum temperature			
	Lowest on record	Decile 1	Decile 10	Highest on record	Lowest on record	Decile 1	Decile 10	Highest on record
Australia	0.00	0.0	42.2	3.71	0.00	0.0	45.7	0.10
Queensland	0.00	0.0	73.1	4.18	0.00	0.0	63.5	0.00
New South Wales	0.00	0.0	91.3	0.00	0.00	0.0	94.5	0.00
Victoria	0.00	0.0	89.9	0.00	0.00	0.0	92.9	3.43
Tasmania	0.00	0.0	79.4	0.00	0.00	0.0	91.9	0.00
South Australia	0.00	0.0	56.4	3.50	0.00	0.0	65.6	0.00
Western Australia	0.00	0.0	0.0	0.00	0.00	0.0	10.0	0.00
Northern Territory	0.00	0.0	30.2	13.44	0.00	0.0	34.3	0.00

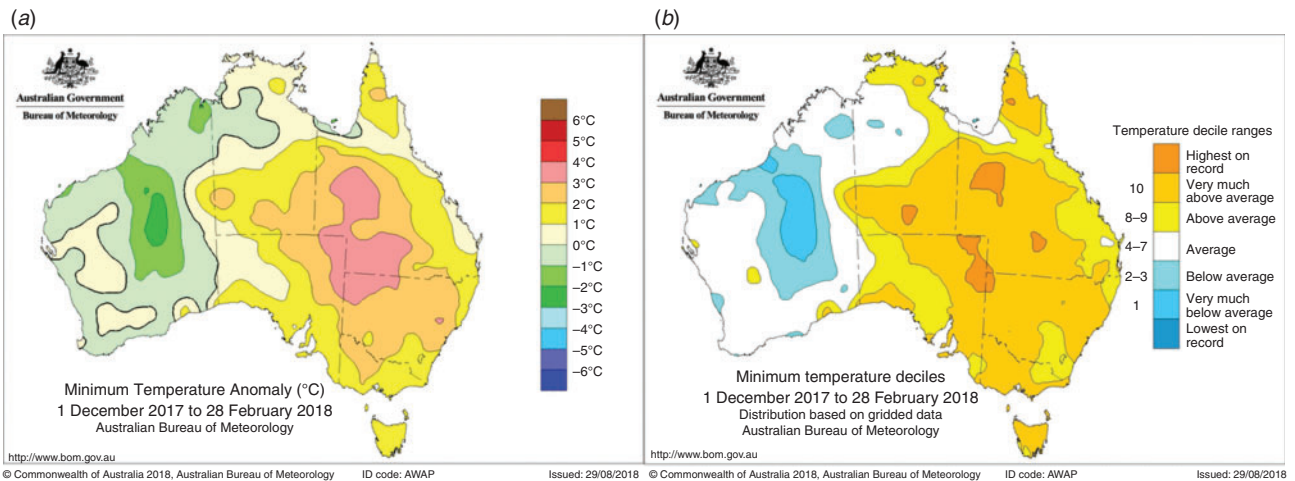


**Fig. 20.** (a) Maximum temperature anomalies ( $^{\circ}\text{C}$ ) for summer 2017–18, based on average climate 1960–91. (b) Maximum temperature deciles for summer 2017–18 from the analysis of ACORN-SAT data: decile ranges based on grid-point values over the summers 1910–2018.

New South Wales, north-western New South Wales and south-east Queensland. Table 3 shows the percentage area in different categories for April 2017 to February 2018.

### 8.3 Temperature

Summer 2017–18 was exceptionally warm for Australia. It was the third-warmest summer on record in terms of mean temperature ( $1.18^{\circ}\text{C}$  above the 1961–90 average). All states and territories, except Western Australia, had a mean temperature for the season amongst the 10 warmest on record. Both maximum and minimum temperatures were also very much above average for Australia, with minima the second-warmest on record for summer ( $1.09^{\circ}\text{C}$ ) and maxima the third-warmest on record for summer ( $1.27^{\circ}\text{C}$ ). Table 4 shows the percentage areas in different categories for summer 2017–18.

Daytime temperatures for summer were above average for the eastern States (Queensland, New South Wales, Victoria and Tasmania), South Australia and most of the Northern Territory away from the Victoria River District. Maxima were in the highest 10% of historical observations (decile 10) for most of the

eastern states, the southern half of the Northern Territory and the eastern half and south-west of South Australia. Cooler than average summer mean maxima were observed over the north-west and interior of Western Australia, associated with very much above-average rainfall in this region. Mean minimum temperatures were above to very much above average for large parts of Australia. Figure 20a shows maximum temperature anomalies ( $^{\circ}\text{C}$ ) for summer 2017–18, based on an average climate from 1960 to 1991, and Fig. 20b shows maximum temperature deciles for summer 2017–18 from analysis of ACORN-SAT data: decile ranges based on grid-point values over the summers 1910–2017. Table 5 shows a summary of the mean seasonal maximum temperatures, extremes and rank for Australia and regions for summer 2017–18.

Minima were in the highest 10% of historical observations (decile 10) for large areas of the eastern States, the eastern half of South Australia, south-east of the Northern Territory, and several isolated areas of Western Australia. Mean minimum temperatures were near average along the east coast of Queensland from the central coast, north to the Cape York Peninsula,

**Table 5. Summary of the mean seasonal maximum temperatures, extremes and rank for Australia and regions for summer 2017–18**  
Rank given is 1 (lowest) to 108 (highest) calculated, over the years 1910–2018 inclusive. AWS, automatic weather station

Region	Highest seasonal mean maximum (°C)	Lowest seasonal mean maximum (°C)	Highest daily maximum temperature (°C)	Lowest daily maximum temperature (°C)	Area-averaged Temperature anomaly (°C)	Rank of area-averaged temperature anomaly
Australia	41.3 at Birdsville Airport	13.8 at kunanyi (Mt Wellington)	47.4 at Birdsville on 29 December 2017, at Wudinna Aero on 19 January 2018 and Marree Aero on 22 January 2018	2.3 at kunanyi (Mt Wellington) on 3 December 2017	1.27	107
Queensland	41.3 at Birdsville Airport	27.5 at Frederick Reef	47.4 at Birdsville on 29 December 2017	15.0 at Applethorpe on 2 February 2018	2.07	107
New South Wales	38.4 at Tibooburra Airport	16.3 at Thredbo AWS	47.3 at Penrith Lakes AWS on 7 January 2018	4.6 at Perisher Valley AWS on 4 December 2017	2.57	105
Victoria	33.8 at Mildura Airport	16.0 at Mt Hotham	46.4 at Walpeup on 19 January 2018	3.6 at Mt Baw Baw on 3 December 2017	1.70	104
Tasmania	25.0 at Cressy Research Station	13.8 at kunanyi (Mt Wellington)	39.7 at St Helens Aerodrome on 19 January 2018	2.3 at kunanyi (Mt Wellington) on 3 December 2017	1.28	100
South Australia	39.8 at Moomba	22.7 at Neptune Island	47.4 at Wudinna Aero on 19 January 2018 and Marree Aero on 22 January 2018	12.1 at Mt Lofty on 7 December 2017	1.95	106
Western Australia	39.5 at Marble Bar	22.3 at Albany	46.7 at Onslow Airport on 24 December 2017	15.4 at Mount Barker on 6 December 2017	0.09	=66
Northern Territory	40.0 at Walungurru Airport	31.8 at McCluer Island	45.8 at Jervois on 29 December 2017	24.5 at Batchelor Airport on 29 January 2018	1.10	=99

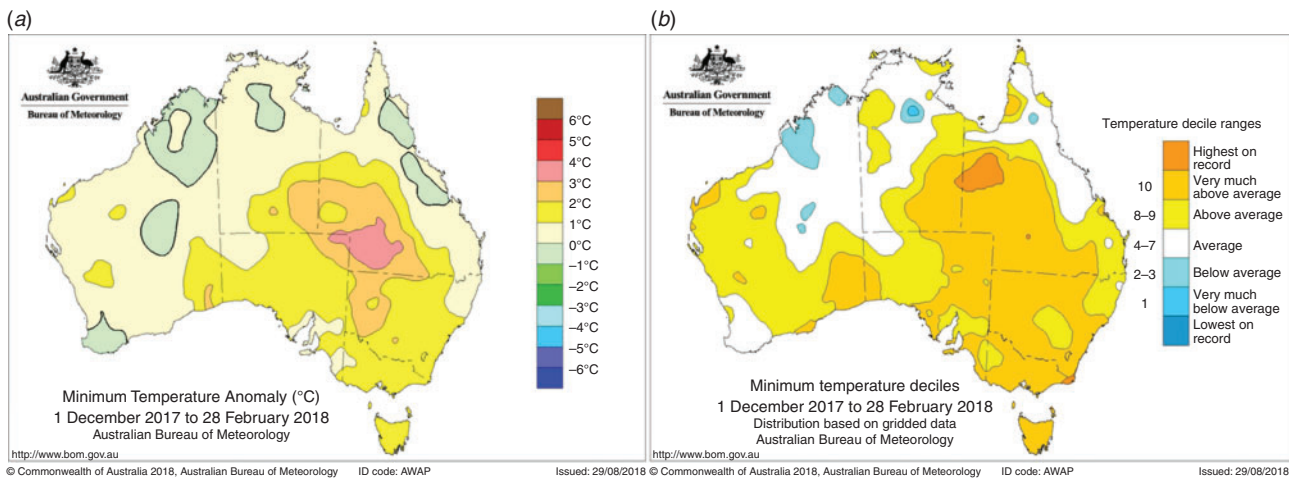


**Fig. 21.** (a) Minimum temperature anomalies (°C) for summer 2017–18; based on average climate 1960–91. (b) Minimum temperature deciles for summer 2017–18 from the analysis of ACORN-SAT data: decile ranges based on grid-point values over the summers 1910–2018.

across most of the north and west of the Northern Territory and in the Kimberley, as well as the Interior and South West districts in Western Australia. Figure 21a shows minimum temperature anomalies (°C) for summer 2017–18, based on an average climate from 1960 to 1991, and Fig. 21b shows minimum temperature deciles for summer 2017–18 from the analysis of

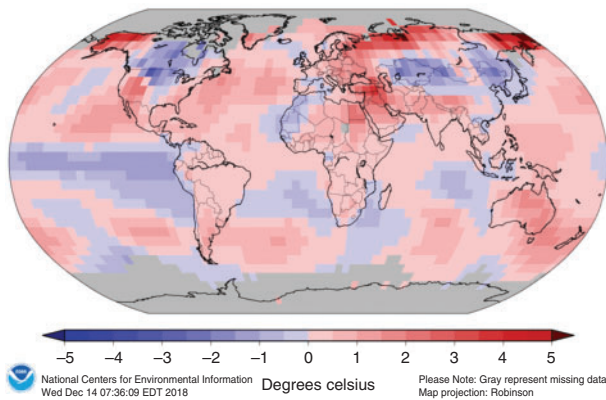
ACORN-SAT data: decile ranges based on grid-point values over the summers 1910–2017.

Each of the individual months of summer were warmer than average nationally. Summer's exceptional warmth was characterised by prolonged, widespread, low-intensity warmth. This included some periods of very warm weather including in

**Table 6. Summary of the mean seasonal minimum temperatures, extremes and rank for Australia and regions for summer 2017–18**  
Rank refers to 1 (lowest)–108 (highest) calculated, over the years 1910–2018 inclusive<sup>8</sup>

Region	Highest seasonal mean minimum (°C)	Lowest seasonal mean minimum (°C)	Highest daily minimum temperature (°C)	Lowest daily minimum temperature (°C)	Area-averaged temperature anomaly (°C)	Rank of area-averaged temperature anomaly
Australia	27.3 at McCluer Island	2.9 at Liawenee	32.0 at Wittenoom and Onslow Airport on 4 March	−9.7 at Cooma Airport on 30 May	1.09	108
Queensland	26.5 at Coconut Island	10.7 at Applethorpe	30.4 at Ballera on 1 March	−4.4 at Stanthorpe on 24 May	1.55	106
New South Wales	18.8 at Byron Bay	3.0 at Perisher Valley	30.5 at White Cliffs on 10 March	−9.7 at Cooma Airport on 30 May	1.94	105
Victoria	17.8 at Mildura Airport	7.9 at Mt Hotham	31.4 at Mildura Airport on 29 January 2018	−2.5 at Mt Hotham on 1 February 2018	1.84	106
Tasmania	15.4 at Swan Island	5.0 at kunanyi (Mt Wellington)	23.9 at Hobart (Ellerslie Road) and Campania (Kincora), both on 29 January 2018	−2.3 at Liawenee on 17 December 2017	1.13	104
South Australia	24.8 at Moomba Airport	11.7 at Keith (Munkora)	34.2 at Marree Aero on 29 January 2018	3.4 at Keith (Munkora) on 25 December 2017	1.41	=104
Western Australia	27.1 at Bedout Island	11.4 at Jarrahwood	33.0 at Wiluna Aero on 5 January 2018	2.5 at Jarrahwood on 1 December 2017	0.34	89
Northern Territory	27.1 at Centre Island	21.6 Arltunga	32.5 at Jervis on 29 December 2017	10.0 at Arltunga on 5 December 2017	0.99	106

Land and Ocean temperature departure from average December 2017–February 2018 (with respect to a 1981–2010 base period)  
Data Source: GHCN–M version 3.3.0 & ERSST version 4.0.0



GPCC Monitoring Product Version 6 Gauge–Based Analysis 1.0 degree precipitation percentage of normals 1951–2000 for Season (December, January, February) 2017–2018 (grid based)

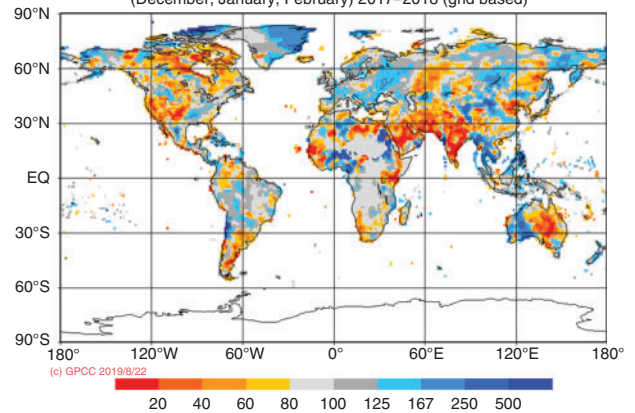


**Fig. 22.** (Left) Global temperature anomalies from 1981 to 2010 base period for December 2017–February 2018 (source: National Oceanic and Atmospheric Administration); (Right) Global precipitation percentage of normal (1951–2000 base period) for December 2017–February 2018 (source: Global Precipitation Climatology Centre).

December, when records were set at multiple stations in New South Wales and South Australia, and in early January around the Sydney region when Penrith Lakes reached 47.3°C on the 7th, which was Greater Sydney’s second-warmest day on record

for any time of year. In northern Tasmania at the end of January, multiple stations set summer records for highest daily minimum temperature, with a few stations also setting records in Victoria. A prolonged warm spell during February saw a number of

<sup>8</sup>A subset of the full temperature network is used to calculate the spatial averages and rankings shown in Table 3 (maximum temperature), Table 4 (minimum temperature) and Table 5; this dataset is known as ACORN-SAT (see <http://www.bom.gov.au/climate/change/acorn-sat/>, verified 29 April 2020 for details). These averages are available from 1910 to the present. As the anomaly averages in the tables are only retained to two decimal places, tied rankings are possible. Rankings marked with ‘=’ denote tied rankings.

stations in Queensland set February records, and on the 12th, Queensland observed its warmest February day on record in terms of area-averaged temperatures, with a state-wide mean maximum temperature of 40.46°C. Table 6 shows a summary of the mean seasonal minimum temperatures, extremes and rank for Australia and regions for summer 2017–18.

### 9 Southern hemisphere

The austral summer of 2017–18 was warmer than average over the southern hemisphere overall. Averages over the hemisphere as a whole, of the three major global data sets, it was the equal ninth-warmest in the National Oceanic and Atmospheric Administration (NOAA) data set (Smith and Reynolds 2005), equal 12th-warmest in the National Air and Space Administration (NASA) data set (Hansen *et al.* 2010) and 16th-warmest in the United Kingdom Meteorological Office Hadley Centre/ Climatic Research Unit, University of East Anglia (HadCRUT) data set (Morice *et al.* 2012).<sup>9</sup> Although temperatures were warmer than average, due to the weak La Niña, it was the coolest since 2011–12 in HadCRUT and the equal coolest with 2013–14 in the NASA data set.

Figure 22 shows global temperature anomalies for December 2017–February 2018. Temperatures over land were above average across much South America, South Africa, Australia and New Zealand. Above-average temperatures were evident over the western to central Pacific, and especially warm in the Tasman Sea. Warmer than usual temperatures were also present off the west and east coasts of South America. Cooler than usual summer temperatures can be seen off the west and east coasts of South Africa, and off the far north-west coast of Australia.

Dry conditions in Argentina and Uruguay and in western South Africa are evident in the global precipitation map (Fig. 22). These areas were associated with high-impact droughts and had damaging agricultural impacts on maize harvests in South America, especially Argentina and Brazil.<sup>10</sup> In South Africa, by January 2018, the reduced rainfall over South Africa had impacts on the availability of drinking water. These areas, along with much of the eastern half of Australia, had below-average summer precipitation. Areas of Chile and Ecuador in South America, the east coast of South Africa, Western Australia and New Zealand had above-average precipitation in summer 2017–18.

### Acknowledgements

The author would like to thank David John Martin and Yanhui Blockley for reviewing early drafts and providing helpful comments that greatly improved this manuscript. This research did not receive any specific funding.

### References

- Hansen, J., Ruedy, R., Sato, M., and Lo, K. (2010). Global surface temperature change. *Rev. Geophys.* **48**, RG4004. doi:10.1029/2010RG000345
- Jones, D. A., Wang, W., and Fawcett, R. (2009). High-quality spatial climate data-sets for Australia. *Aust. Met. Oceanogr. J.* **58**, 233–248
- Kanamitsu, M., Ebisuzaki, W., Woollen, J., Yang, S.-K., Hnilo, J. J., Fiorino, M., and Potter, G. L. (2002). NCEP-DOE AMIP-II Reanalysis (R-2). *Bull. Am. Meteorol. Soc.* **83**, 1631–1643. doi:10.1175/BAMS-83-11-1631
- Kuleshov, Y., Qi, L., Fawcett, R., and Jones, D. (2009). Improving preparedness to natural hazards: tropical cyclone prediction for the Southern Hemisphere. *Adv. Geosci.* **12**(Ocean Science), 127–143.
- Madden, R. A., and Julian, P. R. (1971). Detection of a 40–50 day oscillation in the zonal wind in the tropical Pacific. *J. Atmos. Sci.* **28**, 702–708. doi:10.1175/1520-0469(1971)028<0702:DOADOI>2.0.CO;2
- Madden, R. A., and Julian, P. R. (1972). Description of global-scale circulation cells in the tropics with a 40–50 day period. *J. Atmos. Sci.* **29**, 1109–11023. doi:10.1175/1520-0469(1972)029<1109:DOGSCC>2.0.CO;2
- Madden, R. A., and Julian, P. R. (1994). Observations of the 40–50 day tropical oscillation: a review. *Mon. Wea. Rev.* **122**, 814–837. doi:10.1175/1520-0493(1994)122<0814:OOTDIO>2.0.CO;2
- Morice, C. P., Kennedy, J. J., Rayner, N. A., and Jones, P. D. (2012). Quantifying uncertainties in global and regional temperature change using an ensemble of observational estimates: the HadCRUT4 dataset. *J. Geophys. Res.* **117**, D08101. doi:10.1029/2011JD017187
- Smith, T. M., and Reynolds, R. W. (2005). A global merged land air and sea surface temperature reconstruction based on historical observations (1880–1997). *J. Climate* **18**, 2021–2036. doi:10.1175/JCLI3362.1
- Troup, A. (1965). The Southern Oscillation. *Q. J. R. Meteorol. Soc.* **91**, 490–506. doi:10.1002/QJ.49709139009
- Wang, G., and Hendon, H. H. (2007). Sensitivity of Australian rainfall to inter-El Niño variations. *J. Clim.* **20**, 4211–4226. doi:10.1175/JCLI4228.1
- Wheeler, M., and Hendon, H. (2004). An all-season real-time multivariate MJO index: development of an index for monitoring and prediction. *Aust. Mon. Wea. Rev.* **132**, 1917–1932. doi:10.1175/1520-0493(2004)132<1917:AARMMI>2.0.CO;2

<sup>9</sup>These rankings use the operational data set versions as of July 2019. In some cases the rankings differ from those reported at the time of using earlier data set versions.

<sup>10</sup>The WMO State of the Climate 2018 report ([https://library.wmo.int/doc\\_num.php?explnum\\_id=5789](https://library.wmo.int/doc_num.php?explnum_id=5789), verified 29 April 2020) discusses global impacts in more detail.